Accepted Manuscript

Highly Efficient Polyaniline-MoS_2 Hybrid Nanostructures Based Biosensor for Cancer Biomarker Detection

Amrita Soni, Chandra Mouli Pandey, Manoj Kumar Pandey, Gajjala Sumana

PII: S0003-2670(18)31482-X

DOI: https://doi.org/10.1016/j.aca.2018.12.033

Reference: ACA 236472

To appear in: *Analytica Chimica Acta*

Received Date: 1 October 2018

Revised Date: 11 December 2018

Accepted Date: 14 December 2018

Please cite this article as: A. Soni, C.M. Pandey, M.K. Pandey, G. Sumana, Highly Efficient Polyaniline-MoS_2 Hybrid Nanostructures Based Biosensor for Cancer Biomarker Detection, *Analytica Chimica Acta*, https://doi.org/10.1016/j.aca.2018.12.033.

Graphical Abstract

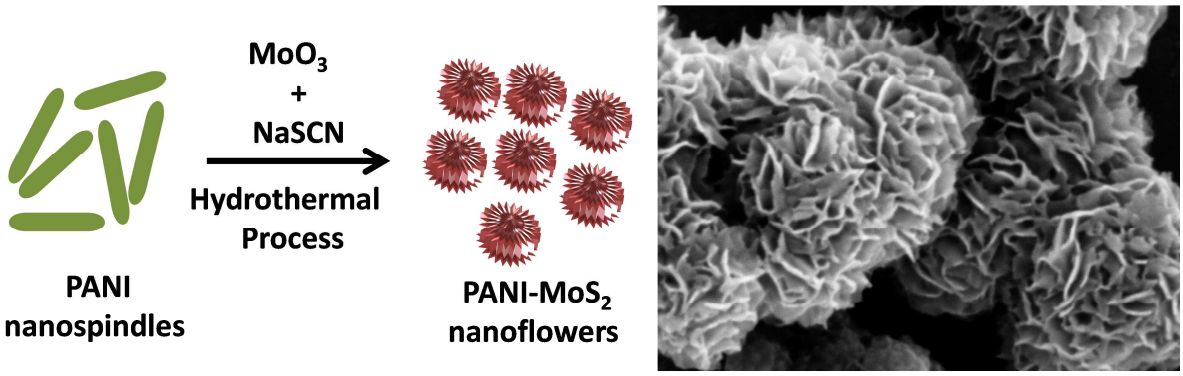

Highly Efficient Polyaniline-MoS_2 Hybrid Nanostructures Based Biosensor for Cancer Biomarker Detection

Amrita Soni[a,b], Chandra Mouli Pandey[c], Manoj Kumar Pandey[b], Gajjala Sumana[b*]

[a]Academy of Scientific and Innovative Research (AcSIR), CSIR-National Physical Laboratory New Delhi-110012, India

[b]CSIR-National Physical Laboratory, New Delhi-110012, India.

[c]Department of Applied Chemistry, Delhi Technological University, Delhi 110042, India

Phone: +91-11-42342439 ; E-mail: sumanagajjala@gmail.com

ABSTRACT

In this work, polyaniline nanospindles have been synthesized using iron oxide as sacrificial template. These nanospindles were utilized for the fabrication of PANI-MoS_2 nanoflower architectures *via* hydrothermal route. The electrostatic interaction between PANI and MoS_2 improves the conductivity and provide more direct paths for charge transportation. SEM, TEM, XRD, Raman Spectroscopy techniques were employed to explore the crystal structure, and morphological properties of the PANI-MoS_2 nanocomposite. Furthermore, an electrochemical biosensing platform based on PANI-MoS_2 nanocomposite was fabricated for the specific detection of chronic myelogenous leukemia (CML) by using electrochemical impedance spectroscopy technique. The binding interactions between the pDNA/PANI-MoS_2/ITO bioelectrode and target DNA sequence were also studied. The biosensor exhibits high sensitivity and wide detection range (10^{-6} M to 10^{-17} M) of target DNA with low detection limit (3×10^{-18} M). Additionally, the specificity studies of the genosensor with various target DNA sequences (complementary, noncomplementary and one base mismatch) and real samples analysis of CML shows its potential for clinical diagnostics.

Keywords: Polyaniline-MoS_2, hybrid structures, electrochemical, cancer, biosensor

1. INTRODUCTION

Recently, transition metal disulfides such as molybdenum disulfide (MoS_2) have attracted tremendous attention in various nanoelectronic, catalysis and electroanalysis field applications due to their large specific areas, unique magnetic and electrochemical properties [1-4]. However, restacking and electrical conductivity of MoS_2 is still a problem, that can be prevented by doping it with conducting polymers [5, 6]. In this regard, polyaniline (PANI) has been used extensively due to its abundant protonated active sites and structural stability during the charge-discharge process[7-9]. Additionally, the nanostructured forms of PANI provide enhanced active surface area and excellent adsorption ability [10, 11]. Though poor mechanical strength, insolubility and bad processability of PANI limit its applications therefore composite of PANI with MoS_2 will overcome the drawbacks coming from the individual counterparts. Moreover, strong coordination bond of metal Mo with nitrogen atoms present in PANI facilitate the controlled growth of MoS_2 on the surface of PANI. Thus, the synergistic effect between MoS_2 and PANI make PANI-MoS_2 nanocomposite an exciting substrate for various fields applications and provides excellent electrocatalytic ability and more paths for insertion and extraction of ions [12].

The electrochemical performance of the material synthesized depends significantly on the morphologies, compositions, surface properties, and their electrical conductivity etc. [13, 14]. Therefore, hybrid nanostructures of PANI-MoS_2 have been introduced as an electrode material for fabrication of the biosensor. Although the exploration of this composite in the field of biosensing is in its primary stage but can be considered as a reliable electrode material for future fabrication of biosensors. For instance, Tao Yang *et al.* demonstrated the polymerization of aniline on the surface of thin layered MoS_2 sheets using a simple ultrasonic exfoliation method. The composite exhibited superior electrochemical performance and utilized for direct and label-free electrochemical DNA sensing with high probe DNA surface coverage area [15]. The PANI-MoS_2 nanocomposite prepared through intercalation of self-doped PANI into the molybdenum disulfide (MoS_2) nanosheets has also been reported. The existence of negative charge and strong π–π^* interactions in the nanocomposite has been employed for label-free detection of single nucleotide (adenine and guanine and their mixture in Britton-Robinson buffer solution) polymorphisms of oligonucleotides [16]. Therefore, hybrid composites can be expected to exhibit improved electrical conductivity and excellent electrochemical performance by

employing the advantages of interfacial interactions between both the materials (PANI and MoS_2).

Chronic Myelogenous Leukemia (CML) is one of the most common types of leukemia, induced by reciprocal translocation of Abelson murine leukemia (ABL) viral oncogene from its normal position (q34) on chromosome 9 to a breakpoint cluster region (BCR) on chromosome 22 (q11), which leads to formation of BCR-ABL fusion gene and the abnormal chromosome is known as Philadelphia (Ph) chromosome [17]. Thus, for the effective treatment of this disease, sensitive and accurate diagnosis is crucial particularly, after the bone marrow transplantation. In recent years, the conventional methods like chromosome analysis, fluorescence in situ hybridization, flow cytometry, and real-time quantitative reverse transcription PCR have been widely used for the detection and prognosis of BCR-ABL fusion gene of CML. Nevertheless, these methods have some disadvantages in terms of time consumption, poor precision, need for high technology instrumentations and expensiveness [18, 19]. Hence, there is still a requirement to develop simple, fast and economical methods for early and accurate detection of BCR/ABL fusion gene. In this context, electrochemical DNA biosensors based on nucleic acid hybridization have been explored extensively owing to their better specificity, response time, portability, regeneration ability and direct diagnosis of blood cancer, tissue matching and various genetic disorders [20] compared to other immunosensors and cells based biosensors[21]. Chen *et al.* have reported an electrochemical biosensor based on graphene sheets/polyaniline/AuNPs nanocomposites for the detection of BCR/ABL fusion gene. The sensor exhibited a detection limit of 1.05×10^{-12}M and was successfully applied for real samples analysis [22]. More recently, in another approach, multiple layer CdS QDs functionalized polystyrene microspheres have been used for signal amplification and graphene oxide-polyaniline composite as an electrode material for the electrochemical detection of K562 cell line, which provides increased detection signal intensity and tumor cells load ratio [23].

In this manuscript, for the first time, we have used polyaniline-nanospindles (PANI-NS) as a substrate for the production of edge-rich integrative 3D hybrid PANI-MoS_2 nanoflowers which were used for the fabrication of high sensitive electrochemical genosensor for CML detection. The sacrificial oxidative Fe_2O_3 template has been used for the synthesis of PANI-NS, which were further utilized as a conductive substrate for the uniform growth of PANI-MoS_2 nanocomposite. The nanocomposite shows excellent properties such as large electroactive

surface area, outstanding conductivity and thus can be used as electrode material for fabrication of electrochemical DNA biosensor.

2. EXPERIMENTAL SECTION

2.1 Reagents and Chemicals

Ferric chloride ($FeCl_3$), hydrochloric acid (HCl), molybdenum trioxide (MoO_3), avidin, sodium thiocyanate (NaSCN), 1-Ethyl-3-(3-dimethylaminopropyl) carbodiimide (EDC), N-Hydroxy succinimide (NHS), ethylene diamine tetra acetic acid (EDTA), monosodium phosphate (NaH_2PO_4), potassium monohydrogen phosphate, potassium dihydrogen phosphate, sodium dodecyl sulfate (SDS), ammonium persulfate (APS), CML-specific oligonucleotide sequences (22 bases; UID no. 12859844) correspond specifically to P210 kDa bcr-abl gene of Philadelphia chromosome,[24] complementary, noncomplementary, one base- mismatch, and all other reagents and solvents have been procured from Sigma-Aldrich Milwaukee, WI. All other chemicals were of analytical grade and used without purification. For the preparation of aqueous solutions, deionized water (D.I; resistance 18.2 MΩ cm) was used. DNA sequences used for the studies are as follows:

Probe DNA: biotin-5'-TGTCCACAGCATTCCGCTGACC-3'

Complementary DNA: 5'-GGTCAGCGGAATGCTGTGGACA-3'

One-base mismatch DNA: 5'-GCTCAGCGGAATGCTGTGGACA- 3'

Non-complementary DNA: 5'-TACTCGCAATAACGTGATCTCC-3'.

2.2 Apparatus and Measurements

Transmission electron microscope (TEM, Hitachi Model, H-800) has been utilized to characterize the Fe_2O_3, PANI-NS, and PANI-MoS_2 nanocomposite. The morphological investigations have been carried out using field emission scanning electron microscope (FESEM, Carl Zeiss). For elemental analysis of the synthesized materials, SEM equipped with an Energy Dispersive X-ray spectroscopy (INCA energy 250 EDX) analyzer has been used. X-ray diffraction (XRD, Rigaku Miniflex X-ray diffractometer) patterns were recorded in the 2θ range with a scan speed of 2°/min using Cu K_α radiation (λ=0.1542nm). Electronic conductivity was measured on compacted pellets using two probe conductivity method. Raman spectra were measured using a 542nm laser, Renishaw via Raman spectrometer. Dynamic light scattering

(DLS) measurements were performed at 25°C with a Zetasizer Nano-ZS90 (Malvern Instruments) at a scattering angle of 90° to determine the zeta potential value of the materials prepared. Fourier Transform Infrared (FT-IR) spectroscopic studies were recorded using Perkin-Elmer spectrometer (model Spectrum BX) at 25°C. Contact angle (CA) studies have been recorded using contact angle meter (Data Physics OCA15EC). Electrochemical measurements have been performed with an Autolab potentiostat/galvanostat (Eco Chemie, Utrecht, The Netherlands) using a conventional three-electrodes system with PANI-NS/ITO or PANI-MoS_2/ITO as working electrode, Pt as an auxiliary electrode and Ag/AgCl as a reference electrode in phosphate buffer (PBS, 100mM, pH 7.0, 0.9% NaCl) containing 5mM of $[Fe(CN)6]^{3-/4-}$.

2.3 Processing of real patient samples

The clinical samples of two male patients (P1 and P2) of Indian origin having 2nd stage CML with age of 33 years and 56 years, respectively were obtained from Rajiv Gandhi Cancer Institute and Research Centre, Delhi, India after the ethical approval by the Institutional Review board (Nos. RGCIRC/IRB/96/2015). For the utilization of CML-positive patients samples in biosensing application prior processing was done by using QIAamp RNA blood mini-kit (Qiagen) for the extraction of RNA from the blood samples. Then, leukocytes were separated from lysed blood by selective erythrocyte lysis followed by repetitive homogenization and washing. Further, the reverse-transcription of separated RNA to complementary DNA (cDNA) was done by high-capacity cDNA reverse transcription kit (Applied Biosystems). The cDNA was diluted 10 times in TE buffer and heated at 100˚C in a water bath for about 5min followed by chilling in an ice bath and then centrifugation at 12 000rpm for about 10min to get denatured single-stranded DNA was done. To break the long DNA chains into smaller fragments, a sample containing DNA was subjected to sonication at 24kHz frequency for 15min [25].

2.4 Synthesis of Fe_2O_3 and PANI nanospindles

Synthesis of monodispersed Fe_2O_3 nanospindles (Fe_2O_3-NS) was done according to previous reported method with slight modifications (Fig. 1(A)) [26]. Firstly, 40mM solution of $FeCl_3$ was prepared in 100ml of deionized (DI) water. Then 1mM of NaH_2PO_4 was added into it, and the solution was heated at 100°C for 72hr. Further, for the synthesis of polyaniline

nanospindles (Fig. 1(B)), Fe_2O_3-NS was dispersed in 100mL of DI water to which 5.5mM of SDS and 1mM of APS were added and the solution was allowed to stand at room temperature for 14hr. After that, 20µl of aniline and 1M HCl was added to the above mixture with continuous stirring at 4°C for 10h. The obtained green color product was washed with HCl, DI water and ethanol to remove the template (Fe_2O_3). The material was then dried in a vacuum oven at 80°C for 24hr.

2.5 Synthesis of PANI- MoS_2 nanoflowers

For the preparation of 3D hybrid PANI-MoS_2 nanoflowers (Fig. 1(C))[27] 50mg of PANI-NS was dispersed in 50mL of deionized water with stirring for 20min followed by sonication. Then 60mM of MoO_3 and 150mM of NaSCN were added to above PANI-NS suspension and stirred for 30min. The obtained mixture was then transferred to a Teflon-lined stainless steel autoclave and kept at 220°C for 24hr. Subsequently, the obtained black material was washed with DI water and ethanol several times till pH value reaches to 7.0. The product was then dried in a vacuum oven at 80°C for 24hr.

2.6 Preparation of PANI-NS/ITO and PANI-MoS_2/ITO electrodes

Electrophoretic deposition of synthesized PANI-NS and PANI-MoS_2 was successfully done using a two-electrode system. Pre-hydrolyzed ITO (0.5cm^2) substrate has been used for deposition of synthesized material on the surface of ITO which can interact strongly with $–NH_2$ group present in the PANI. For the deposition of the PANI-NS, 10mg of PANI-NS was dispersed in a mixture of ethanol and deionized water (1:1) and 30V was applied for 45s by taking ITO substrate as cathode and thin platinum foil as an anode. Similarly, a colloidal suspension of PANI-MoS_2 was prepared by dispersing 5mg of the composite in 20 ml of acetonitrile with the help of ultrasonication. PANI-MoS_2 was deposited onto ITO electrodes anodically at a DC potential of 40V for 80s with platinum as the counter electrode. The obtained electrodes were rinsed with deionized water three times and then air-dried.

2.7 Functionalization and hybridization of probe DNA

Avidin-Biotin interactions have been utilized for the bioconjugation of the biotinylated pDNA to the surface of electrophoretically deposited PANI-MoS_2/ITO electrodes (Fig. 3(A)).

For this purpose, 20µl of 1mg/mL avidin solution activated by EDC (0.2M) and NHS (0.4M) was immobilized on the surface of PANI-MoS_2/ITO electrodes at 25°C for 2hr. Consecutively, avidin-PANI-MoS_2/ITO electrodes were washed with PB buffer and incubated with 20µl of biotinylated probe DNA having 22 basepairs (1.0µM) for 3.5hr in a humid chamber at room temperature (Fig. 3(A)). The prepared bioelectrodes (pDNA/PANI-MoS_2/ITO) were rinsed with Tris-HCl (10mM) and EDTA (1mM) buffer solution (TE, pH 8.0) several times to remove any unbound pDNA from the electrode surface [28]. The pDNA/PANI-MoS_2/ITO bioelectrodes were further employed for the hybridization studies by incubating it with different concentrations of cDNA sequences (10^{-17}-10^{-6}M), complementary, non-complementary and one-base mismatch DNA sequences for about 15min in a humid chamber at 25°C (Fig. 3(A)). All the DNA solutions were prepared in Tris-EDTA buffer solution.

3. RESULTS AND DISCUSSION

3.1Microscopic and structural analysis

For analyzing the size and structure, which are the key parameters in controlling the chemical and physical performances of the materials synthesized, TEM studies were performed. Figure 1(D) shows a uniform and dense distribution of spindle-like nanostructures of Fe_2O_3 with a lateral dimension of about 50nm having an inter-planar spacing of 0.37Å, which is further confirmed by HRTEM image (Fig. 1(E)). These synthesized spindles like Fe_2O_3 nanostructures may act as a template for the formation of PANI-NS. Polymerization of aniline on the surface of Fe_2O_3-NS and removal of the template leads to the growth of PANI-NS (Fig. 1(F)). Due to flexible nature of PANI and deposition of multiple layers around the surface of Fe_2O_3, PANI-NS get slightly bend from the edges and results in larger lateral dimension in the range of 70-80nm in comparison to Fe_2O_3-NS (Fig. 1(G)).

Further, these highly dispersed PANI-NS worked as nucleation sites for the uniform and stable growth of PANI-MoS_2 nanocomposite. Figure 1(H & I) shows TEM images of the synthesized PANI-MoS_2 nanocomposite, where multiple thin nanosheets of MoS_2 are stacked by covering the complete surface of PANI-NS and formed a 3D hybrid flower-like nanostructures with several folds having diametre in the range of 500- 700nm. HRTEM image (Supplementary material Fig. S1(A)) of PANI-MoS_2 hybrid material represents the lattice fringes with an

interlayer spacing of 0.62nm which is consistent with the 002 planes of MoS_2 nanosheets and denotes a crystalline structure. However, the absence of lattice fringes in PANI depicts it amorphous nature in the hybrid material (Supplementary material Fig. S1(B)).

XRD measurements have been carried out to investigate the crystallographic structure of the materials synthesized. The XRD pattern of the synthesized Fe_2O_3 nanospindles can be seen in Figure S1(C). After polymerization of aniline on the surface of Fe_2O_3 and subsequent removal of Fe_2O_3 causes broadening of the diffraction peaks in the XRD spectrum of PANI-NS (Fig. 2(A)). Moreover, some diffraction peaks which correspond to the Fe_2O_3 can also be observed in the spectrum which is may be due to incomplete removal of the template. Whereas, broadening suggests the existence of PANI in a semicrystalline state which is ascribed to the periodicity perpendicular and parallel to the polymer backbone chain [29]. Further, in the XRD pattern of PANI-MoS_2 (Fig. 2(B)) diffraction peaks observed at 13.8˚, 33.5˚, 40.1˚, 53.5˚ and 59˚ represents the (002), (100), (103), (105) and (110) diffraction planes of MoS_2 respectively, which confirms the well-defined hexagonal structure of MoS_2 while weak diffraction band observed from 16.6 to 30.5˚ is related to the presence of polyaniline [30]. The relative lower intensity of diffraction peak at 13.8˚ signifies that MoS_2 nanosheets may contain only a few layers. The interlayer distance of (002) plane which is the S-Mo-S layer was calculated to be 0.62nm by using the Bragg equation [30].

The Raman spectrum of the PANI-NS (Fig. 2(C); (i)) exhibits peaks at 1609, 1485, 1346, 1190 and 820cm^{-1} which are assigned to C-C stretching vibration of benzenoid ring, C=C stretching vibration of quinoid ring, C-N^+ stretching of polaron structure, C-H bending vibrations and C-N stretching vibration of secondary amine respectively. Whereas, a slight shift in the peak positions assigned to polyaniline can be observed in the Raman spectrum of PANI-MoS_2 nanocomposite (Fig. 2(C); (ii)) compared to Raman spectrum obtained for PANI-NS. The additional two well-resolved peaks at 378 and 403cm^{-1} are ascribed to E^1_{2g} in-plane vibration and A^1_{2g} out-of-plane vibration of Mo and S atoms respectively [31].

3.2 Zeta potential, conductivity and EDX measurements

To determine the magnitude and sign of the effective charge on the surface of PANI-NS, and PANI-MoS_2, zeta potential studies were carried out using the Smoluchowski method [32]. PANI-NS exhibited a positive zeta potential value of 28.5mV (Fig. 2(D)) revealing the presence

of amine and imine groups. Whereas, after formation of a composite with MoS_2, the PANI-MoS_2 nanocomposite exhibited zeta potential value of -26.1mV (Fig. 2(E)), suggesting the electrostatic interaction between negatively charged MoS_2 and positively charged PANI, which decreases the overall charge on the surface of the composite synthesized to a negative value (-26.1mV).

The conductivity of the synthesized PANI-NS and PANI-MoS_2 samples was measured on pellets pressed from powders using two probe method at room temperature. The measured conductivity value of PANI-MoS_2 showed an enhancement of about one order of magnitude in comparison to the conductivity value of PANI-NS and was found to be 8.26×10^{-1}S/cm and 9.31×10^{-2}S/cm respectively. This increase in the conductivity value is explained by large electroactive surface area and increased the degree of conjugation of π bonds of the nanocomposite, which provides low interfacial charge transfer resistance and reduces the ion diffusion length as a result of interfacial interactions between PANI and MoS_2 monolayers [31]. Also, the compact and homogeneous distribution of PANI facilitates fast transportation of π electrons between PANI and MoS_2 that leads to high intrinsic ionic conductivity.

To analyze the elemental composition of the synthesized PANI-MoS_2 nanocomposite, the EDX profile was recorded. The EDX spectrum of PANI-MoS_2 shows the signals corresponding to C, O, N, Mo, and S with their respective weight percentages (Fig. 3(D)). The peak of carbon along with nitrogen represents the existence of polyaniline, while the peaks of Mo and S confirm the presence of MoS_2. The remaining peaks (O, Zr and Na) observed in the spectrum are either due to the doping process or side products formed during hydrothermal process.

3.3 Surface characterization of prepared electrodes and bioelectrode

The morphology of the prepared PANI-NS/ITO, PANI-MoS_2/ITO electrodes and pDNA/PANI-MoS_2/ITO bioelectrode was confirmed by FESEM. The FESEM image of PANI-NS/ITO shows dense particle distribution of nanospindles that leads to tightly interconnection of particles (Fig. 3(B)) However, FESEM image of PANI-MoS_2 reveals completely different, flower-like morphology (Fig. 3(C) and Fig. S1(D)) facilitated by electrostatic interaction between aromatic groups of PANI and basal planes of MoS_2, indicating that PANI act as substrate for the formation of flower-like nanostructures by enfolding MoS_2 on its surface. Some nanoflowers deposited are in isolation while some forms domains and exhibit dense morphology, suitable for improved electrochemical performance and sensor sensitivity [33]. The image at

higher magnification (inset of Fig. 3(C)) clearly shows that nanoflowers have a diameter in the range of 500-700nm which is consistent with the results of TEM and comprises of very thin nanoplates having a thickness of about 15nm. This flower-like nanostructures, due to their large active surface area assist the efficient immobilization of pDNA without creating any steric hindrance. Hence, on incubation of pDNA with PANI-MoS_2/ITO electrode (Fig. 3(E)) globular morphology with shiny appearance indicates that the electrode surface has been covered by pDNA [32], which can be clearly seen in the magnified image (inset Fig. 3(E)). The variation in the morphology reveals the successful attachment of pDNA onto PANI-MoS_2/ITO electrode.

The FT-IR spectra of the PANI-NS/ITO, PANI-MoS_2/ITO electrodes and pDNA/PANI-MoS_2 bioelectrode are shown in Supplementary material Figure S2. The peaks observed at about 794 and 1115cm^{-1} in the curves of PANI-NS/ITO (Supplementary material Fig. S2(A)) and PANI-MoS_2/ITO (Supplementary material Fig. S2(B)) electrodes are related to C-H out of plane bending and in-plane bending of quinoid and benzenoid rings respectively. Peaks are seen at about 1230 and 1292cm^{-1} in both the curves (Supplementary material Fig. S2(A and B)) are attributed to C-N and C**=N** stretching vibrations of the aromatic amine. Whereas, peaks centered at about 1469 and 1560cm^{-1} in both the spectrum are assigned to C=C stretching deformations of benzene and quinone rings respectively. The FT-IR spectrum of both the electrodes (PANI-NS/ITO and PANI-MoS_2/ITO) exhibit the characteristic bands corresponding to PANI except the peak at 570cm^{-1} in the FTIR spectrum of PANI-MoS_2/ITO electrode, that belongs to Mo-S stretching vibration and indicates the successful deposition of the nanocomposite onto ITO electrode [34]. Supplementary material Figure S2(C) shows FT-IR spectrum of the pDNA/PANI-MoS_2 bioelectrode, the additional bands can be seen at 980, 1043, 1377, 1420 and 1627cm^{-1}, among these bands 980, 1043 and 1377cm^{-1} are associated with C-N stretching vibration, anti-symmetric and symmetric stretching vibration modes of P–O–C and P=O in phosphoric acid group respectively and 1420 and 1627cm^{-1} attributed to –CN and carbonyl stretching vibrations existing in the nucleoside bases respectively, indicating the proper immobilization of probe DNA on the surface of PANI-MoS_2/ITO electrode.

To confirm the effective immobilization of the pDNA on the electrode surface, contact angle (CA) studies have been carried out using the sessile drop method [32]. The CA value observed for the bare ITO electrode is 74.8° (Supplementary material Fig. S3(A)), but after the deposition of PANI-NS on ITO electrode the value of CA decreases to 48.2° (Supplementary

material Fig. S3(B)) indicating the availability of hydrophilic amine and imine groups on surface of PANI-NS/ITO electrode. A further decrease in the value of CA for the PANI-MoS_2/ITO electrode to 32.3°(Supplementary material Fig.S3(C)) reveals the introduction of more hydrophilic groups on its surface whether, on immobilization of pDNA on the PANI-MoS_2/ITO using biotin-avidin interactions, CA value decreases to 12.4° for pDNA/PANI-MoS_2/ITO bioelectrode(Supplementary material Fig.S3(D)) which signifies the enhanced hydrophilicity due to presence of phosphodiester backbone of pDNA that can be related to immobilization of the pDNA on electrode surface[35].

3.4 Electrochemical Characterization

Electrochemical studies of the PANI-NS/ITO, PANI-MoS_2/ITO electrodes and pDNA/PANI-MoS_2/ITO bioelectrode have been performed in phosphate buffer saline (100mM, pH 7.0, 0.9% NaCl) containing 5mM of $[Fe(CN)_6]^{3-/4-}$ using cyclic voltammetry (CV) technique at a scan rate of 30mV/sec (Supplementary material Figure S4(A)). The CV of PANI-NS/ITO electrode shows an increase in the peak current value (1.14mA; curve(iv)) in comparison to bare ITO electrode (435.28μA; curve(i)), which further increases to 1.27mA (curve(v)) for the PANI-MoS_2/ITO electrode. This increase in the peak current value for PANI-MoS_2/ITO electrode is attributed to the hybrid structure of PANI-MoS_2 which act as a catalyst and offer abundant sites for the efficient electron transfer through the electrode in the electrochemical cell. After immobilization of pDNA on PANI-MoS_2/ITO electrode, a decrease in the value of peak current (802.34μA; curve(iii)) with respect to PANI-MoS_2/ITO electrode has been observed which decreases further to 659.39μA(curve(ii)) on hybridization with target DNA. This subsequent decrease in the peak current value corresponds to the long polymer chain of DNA that slows the electron transfer through the bioelectrode [25].

To determine the various kinetic parameters the CV studies have been carried out at various potential scan rates (10–300mVs^{-1}) for PANI-NS/ITO (Supplementary material Fig. S4(B)), PANI-MoS_2/ITO electrodes (Supplementary material Fig. S4(C)) and pDNA/PANI-MoS_2/ITO bioelectrode (Supplementary material Fig. S4(D)). It has been observed that on increasing the scan rate, the anodic peak potential shifts to a more positive value and the cathodic peak to a more negative value, revealing a quasi-reversible system. The anodic and cathodic peak currents (I_{pa} and I_{pc}) and potential peak values (E_{pa} and E_{pc}) are proportional to the square root of

scan rate and log of scan rate respectively over the range of 10–300mVs^{-1}, suggesting a diffusion controlled electrochemical process on the modified electrodes. The value of electron transfer coefficient (α) and electron transfer rate constant (K_s) for different electrodes were determined by using Laviron's theory [32] and value of diffusion coefficient(D) and electroactive surface areas(A) were measured by using Randles–Sevcik equation [32]. The calculated kinetic parameters are represented in Supplementary material Table S1. The improvement in kinetic parameters of PANI-MoS_2/ITO electrode compared to PANI-NS/ITO electrode is due to flower like morphology of the PANI-MoS_2 which provides more active edges for the direct charge transfer and increased surface area. Whereas, kinetic parameters calculated for pDNA/PANI-MoS_2/ITO bioelectrode indicates high and uniform surface coverage of pDNA onto the PANI-MoS_2/ITO electrode.

To investigate the interfacial electronic properties between the electrodes before and after surface modification and electrolyte, electrochemical impedance spectroscopy (EIS) measurements have been carried out (0.01-10^5Hz) in the presence of phosphate buffer (100mM, pH 7.0, 0.9% NaCl) and $[Fe(CN)_6]^{3-/4-}$ as a redox marker at working potential of 0.05V. Computer simulated fitting of obtained faradic impedance spectra of PANI-MoS_2/ITO electrode has been done using six different electronic circuits (EC) based on Randles and Ershler theoretical models (Figure S6)[36]. It was observed that good fit between the experimental spectra and the simulated electronic circuit is obtained for EC5- $R_s(C_{dl}[R_{ct}\ Z_W])$. Though, by adding one more R and C elements in EC 5, i.e., EC6- $R_s(R_{ct}1C_{dl}1)\ (C_{dl}2[R_{ct}2\ Z_W])$ a better fit was obtained but percentage error was found higher in comparison to that of EC5- $R_s(C_{dl}[R_{ct}\ Z_W])$ so, EC-5 has been considered as best fit for the experimental data.

The characteristic impedance spectra (Nyquist plots) of the fabricated electrodes (PANI-MoS_2/ITO, PANI-NS/ITO) and bioelectrode (pDNA/PANI-MoS_2/ITO) are illustrated in Figure 4(A) and the Randles equivalent circuit is presented in the inset of Figure 4(A), which contains electron transfer resistance (R_{ct}), Constant phase element (C_{PE}), solution resistance (R_s), and Warburg impedance (Z_w). The values of R_{ct}, C_{PE}, R_s, Z_w for PANI-MoS_2/ITO electrode were found to be 286.4Ω, 11.10μF, 39.6 Ω and $.322\times10^{-1}$ respectively. The change in the electron-transfer resistance which is represented by the diameter of semicircle at electrode−solution interface can be correlated to transfer of electrochemically produced charges[37]. The R_{ct} value of 489.4Ω for the PANI-NS/ITO electrode (Figure 4(A); curve(ii)) is attributed to increased

conductivity which facilitates fast electron transfer. Moreover, a decrease in the value of R_{ct} to 286.4Ω for PANI-MoS_2/ITO electrode (Figure 4(A); curve(i)) is assigned to increased surface area owing to flower like morphology and strong π–π* interactions between the aromatic backbones of PANI and basal planes of MoS_2 which enables direct path for charge transfer and superior electrocatalytic performance [14]. Further, on immobilization of pDNA onto PANI-MoS_2/ITO electrode, the R_{ct} value increases to 1045.8Ω (Figure 4(A); curve(iii)) which is assigned to presence of negatively charged phosphate backbone of pDNA that hinders the electron transfer on the electrode surface by repelling the negatively charged redox marker $[Fe(CN)_6]^{3-/4-}$. Optimization of various experimental conditions (probe concentration, immobilization time and incubation time) has been explained in supplementary material section.

3.5 Electrochemical response studies

DNA hybridization studies have been performed by incubating pDNA/PANI-MoS_2/ITO bioelectrode with varying concentrations (10^{-6} to 10^{-17}M) of the complementary DNA sequence (Figure 4(B)). On incubating the bioelectrode with cDNA, hybridization occurs and the R_{ct} value increases with increase in the concentration of cDNA, indicating the introduction of more negatively charged phosphate backbones of DNA, which repels the $[Fe(CN)_6]^{3-/4-}$ redox ion. The measurement signal ($\Delta R_{ct} = R_{ct}c_{DNA} - R_{ct}p_{DNA}$) exhibited a linear relationship with the logarithmic value of the complementary target DNA concentration ranging from 10^{-17} to 10^{-6}M (Fig. 4(C)) and follows the subsequent equation:

$$\Delta R_{ct} = 8289.03 + 451.26 \log \text{cDNA}$$

with a linear regression coefficient (RC) of 0.9936. The detection limit calculated using the expression 3σ/sensitivity has been found to be 3×10^{-18} M where σ is the standard deviation of the pDNA/PANI-MoS_2/ITO electrode. In addition, to study the binding interactions between pDNA/PANI-MoS_2/ITO bioelectrode and cDNA, the association constant (K_a) was calculated using the Langmuir isotherm approach in which isotherm assumes equal binding energy for all the binding sites [38]. The variation in R_{ct} value was used to determine the K_a and is expressed by the following equation:

$$M = 1 - R_{ct}(pDNA)/R_{ct}(cDNA) \quad (1)$$

Where M, is the number of occupied, binding sites, R_{ct}(pDNA) and R_{ct}(cDNA) is charge transfer resistance of pDNA/PANI-MoS_2/ITO bioelectrode before and after hybridization with cDNA, respectively. The relation between M and K_a can be represented by the following equation:

$$M = K_aC /1+K_aC \quad (2)$$

Where C is the concentration of molecules in the solution

From equations 1 and 2

$$K_aC = R_{ct}(cDNA) – R_{ct}(pDNA) / R_{ct}(pDNA) \quad (3)$$

which can be written as

$$K_aC = \Delta R_{ct} / R_{ct}(pDNA) \quad (4)$$

Using equation 4, the curve between $\Delta R_{ct}/R_{ct}$(pDNA) and concentration of cDNA showed linearity (Supplementary material Fig. S7) and follows the equation

$$\Delta R_{ct}/R_{ct}(pDNA) = 7.0298 + 0.2347 \log cDNA \quad (5)$$

with a correlation coefficient of 0.979. Whereas, K_a for pDNA/PANI-MoS_2/ITO bioelectrode was measured from the slope of the regression equation and was found to be $0.413M^{-1}$. This high value of K_a for flower-like nanostructures corresponds to the conducive morphology which provides abundant sites for loading of pDNA.

3.6 Specificity and validation with real samples

The specificity of the prepared bioelectrode was evaluated by incubating with different target DNA sequences including cDNA, single-base mismatch and non-complementary DNA sequence with pDNA/PANI-MoS_2/ITO bioelectrode under the same experimental conditions (Fig. 4(D)). The significantly higher R_{ct} value of the complementary DNA sequence (6037.6Ω) in comparison to the other two mismatch DNA sequences (one base, non-complementary) showed that the pDNA immobilized onto PANI-MoS_2/ITO electrode has successfully hybridized with its cDNA sequence. Whereas, a very small increase in the R_{ct} value (1106.9Ω) was

observed when pDNA/PANI-MoS_2/ITO bioelectrode was incubated with single-base mismatch DNA sequence illustrating that hybridization occurred incompletely due to mismatching of the DNA sequences. However, after incubating the pDNA/PANI-MoS_2/ITO bioelectrode with non-complementary DNA sequences, no obvious change in the R_{ct} value (970.5Ω) was observed showing the little or no hybridization has taken place.

To test the real application of the fabricated biosensor, the change in R_{ct} value of the bioelectrode after hybridization with real samples of CML patients was determined (Fig. 4(D)). It was observed that the R_{ct} values obtained for the CML positive patient samples are similar to the R_{ct} value of cDNA, which shows complete hybridization with pDNA sequence. These results demonstrate that the biosensor exhibits high specificity for synthetic as well as real samples of CML patients. The performance of the fabricated biosensor compared to other biosensors reported for CML detection has been summarized in Supplementary material Table S2. It was observed that the fabricated biosensor exhibits enhanced sensitivity and stability compared to other biosensors.

3.7 Stability, reproducibility and regeneration studies

The fabricated biosensor was found to have high stability of 6 weeks and retained 87.5% of its original signal response after eight cycles of successive denaturation and regeneration with reasonably good repeatability(details can be found in supplementary material section).

4. CONCLUSIONS

In summary, a facile strategy has been presented for the synthesis of PANI-NS by using Fe_2O_3 as the oxidative sacrificial template. Thereafter, PANI-NS have been used as a substrate for the construction of 3D hybrid PANI-MoS_2 nanoflowers via hydrothermal route. The unique architecture of PANI-MoS_2 offers large electroactive surface area, fast electron transportation and improved catalytic activity, which are advantageous for the enhancement of electrochemical performance. Further, PANI-MoS_2 composite has been employed as a sensing platform for the detection of CML over a wide range of target DNA concentration (10^{-6}-10^{-17}M). The fabricated genosensor has a low limit of detection (3×10^{-18} M), good regeneration capability and high stability for 42days (at 4°C) and was also able to detect CML in the clinical samples. With these outstanding benefits facilitated by a synergistic effect between MoS_2 and PANI, this biosensor

platform might also be used in other electrochemical sensors, electro-analysis of biological and organic molecules and may have implications in new generation point of care diagnostics.

ACKNOWLEDGEMENTS

We are thankful to Director, National Physical Laboratory, India for providing facilities. A.S. is grateful to CSIR, India, for the award of SRF. C.M.Pandey acknowledges the financial support received from Department of Science and Technology, India under DST-INSPIRE Faculty Project (Grant No. DST/INSPIRE/04/2015/000932). We extend our thanks to Prof. B.D Malhotra for his valuable discussions. Author thanks Dr. Birendra Kumar Yadav (Rajiv Gandhi Cancer Institute and Research Centre, New Delhi) for providing the clinical patient samples.

REFERENCES

[1] L. Yang, D. Zhong, J. Zhang, Z. Yan, S. Ge, P. Du, J. Jiang, D. Sun, X. Wu, Z. Fan, Optical properties of metal-molybdenum disulfide hybrid nanosheets and their application for enhanced photocatalytic hydrogen evolution, ACS nano, 8 (2014) 6979-6985.

[2] S. Solanki, A. Soni, M.K. Pandey, A. Biradar, G. Sumana, Langmuir-Blodgett Nanoassemblies of the MoS_2-Au Composite at the Air-Water Interface for Dengue Detection, ACS appl. mater. interfaces, 10 (2018) 3020-3028.

[3] Z. Zheng, Q. Feng, J. Li, C. Wang, The p-type MoS_2 nanocube modified poly (diallyl dimethyl ammonium chloride)-mesoporous carbon composites as a catalytic amplification platform for electrochemical detection of L-cysteine, Sens. Actuators B: Chem., 221 (2015) 1162-1169.

[4] K.-J. Huang, J.-Z. Zhang, G.-W. Shi, Y.-M. Liu, Hydrothermal synthesis of molybdenum disulfide nanosheets as supercapacitors electrode material, Electrochim. Acta, 132 (2014) 397-403.

[5] N. Zhang, W. Ma, T. Wu, H. Wang, D. Han, L. Niu, Edge-rich MoS_2 naonosheets rooting into polyaniline nanofibers as effective catalyst for electrochemical hydrogen evolution, Electrochim. Acta, 180 (2015) 155-163.

[6] X. Wang, W. Xing, X. Feng, L. Song, Y. Hu, MoS2/Polymer nanocomposites: preparation, properties, and applications, Poly. Rev., 57 (2017) 440-466.

[7] H.-W. Park, T. Kim, J. Huh, M. Kang, J.E. Lee, H. Yoon, Anisotropic growth control of polyaniline nanostructures and their morphology-dependent electrochemical characteristics, ACS nano, 6 (2012) 7624-7633.

[8] R. Ramya, R. Sivasubramanian, M.V. Sangaranarayanan, Conducting polymers-based electrochemical supercapacitors- progress and prospects, Electrochim. Acta, 101 (2013) 109-129.

[9] E. Song, J.-W. Choi, Conducting polyaniline nanowire and its applications in chemiresistive sensing, Nanomaterials, 3 (2013) 498-523.

[10] Y. Shi, M. Wang, C. Ma, Y. Wang, X. Li, G. Yu, A conductive self-healing hybrid gel enabled by metal-ligand supramolecule and nanostructured conductive polymer, Nano letters, 15 (2015) 6276-6281.

[11] L. Peponi, D. Puglia, L. Torre, L. Valentini, J.M. Kenny, Processing of nanostructured polymers and advanced polymeric based nanocomposites, Mat. Sci. Eng. R, 85 (2014) 1-46.

[12] H. Wang, H. Jiang, Y. Hu, N. Li, X. Zhao, C. Li, 2D MoS_2/polyaniline heterostructures with enlarged interlayer spacing for superior lithium and sodium storage, J. Mater. Chem. A, 5 (2017) 5383-5389.

[13] Z. Liu, X. Wang, P. Qiao, Y. Tian, H. Li, J. Yang, Uniformed polyaniline supported MoS_2 nanorod: a photocatalytic hydrogen evolution and anti-bacteria material, J. Mater Sci: Mater. El. 26 (2015) 7153-7158.

[14] J. Lei, Z. Jiang, X. Lu, G. Nie, C. Wang, Synthesis of few-layer MoS_2 nanosheets-wrapped polyaniline hierarchical nanostructures for enhanced electrochemical capacitance performance, Electrochim. Acta, 176 (2015) 149-155.

[15] T. Yang, L. Meng, H. Chen, S. Luo, W. Li, K. Jiao, Synthesis of Thin-Layered Molybdenum Disulfide-Based Polyaniline Nanointerfaces for Enhanced Direct Electrochemical DNA Detection, Adv. Mater Interfaces, 3 (2016).

[16] T. Yang, R. Yang, H. Chen, F. Nan, T. Ge, K. Jiao, Electrocatalytic activity of molybdenum disulfide nanosheets enhanced by self-doped polyaniline for highly sensitive and synergistic determination of adenine and guanine, ACS appl. mater. interfaces, 7 (2015) 2867-2872.

[17] S. Chu, H. Xu, N.P. Shah, D.S. Snyder, S.J. Forman, C.L. Sawyers, R. Bhatia, Detection of BCR-ABL kinase mutations in CD34+ cells from chronic myelogenous leukemia patients in complete cytogenetic remission on imatinib mesylate treatment, Blood, 105 (2005) 2093-2098.

[18] M.A. Tainsky, Genomic and proteomic biomarkers for cancer: a multitude of opportunities, Biochim. Biophys. Acta, 1796 (2009) 176-193.
[19] M. Shamsipur, V. Nasirian, A. Barati, K. Mansouri, A. Vaisi-Raygani, S. Kashanian, Determination of cDNA encoding BCR/ABL fusion gene in patients with chronic myelogenous leukemia using a novel FRET-based quantum dots-DNA nanosensor, Anal. chim. acta, 966 (2017) 62-70.
[20] C.M. Pandey, S. Dewan, S. Chawla, B.K. Yadav, G. Sumana, B.D. Malhotra, Controlled deposition of functionalized silica coated zinc oxide nano-assemblies at the air/water interface for blood cancer detection, Anal. chim. acta, 937 (2016) 29-38.
[21] V. Kavita, DNA biosensors-a review, J. Bioengineer & Biomedical Sci., 7 (2017).
[22] X. Chen, L. Wang, S. Sheng, T. Wang, J. Yang, G. Xie, W. Feng, Coupling a universal DNA circuit with graphene sheets/polyaniline/AuNPs nanocomposites for the detection of BCR/ABL fusion gene, Anal. chim. acta, 889 (2015) 90-97.
[23] J. Wang, X. Wang, H. Tang, Z. Gao, S. He, J. Li, S. Han, Ultrasensitive electrochemical detection of tumor cells based on multiple layer CdS quantum dots-functionalized polystyrene microspheres and graphene oxide-polyaniline composite, Biosen Bioelectron, 100 (2018) 1-7.
[24] A. Sharma, C.M. Pandey, G. Sumana, U. Soni, S. Sapra, A.K. Srivastava, T. Chatterjee, B.D. Malhotra, Chitosan encapsulated quantum dots platform for leukemia detection, Biosen Bioelectron, 38 (2012) 107-113.
[25] A. Soni, C.M. Pandey, S. Solanki, R.K. Kotnala, G. Sumana, Electrochemical genosensor based on template assisted synthesized polyaniline nanotubes for chronic myelogenous leukemia detection, Talanta, 187 (2018) 379-389.
[26] C.-L. Zhu, S.-W. Chou, S.-F. He, W.-N. Liao, C.-C. Chen, Synthesis of core/shell metal oxide/polyaniline nanocomposites and hollow polyaniline capsules, Nanotechnology, 18 (2007) 275604.
[27] L. Hu, Y. Ren, H. Yang, Q. Xu, Fabrication of 3D hierarchical MoS_2/polyaniline and MoS2/C architectures for lithium-ion battery applications, ACS appl. mater. interfaces, 6 (2014) 14644-14652.
[28] R. Singh, R. Verma, G. Sumana, A.K. Srivastava, S. Sood, R.K. Gupta, B.D. Malhotra, Nanobiocomposite platform based on polyaniline-iron oxide-carbon nanotubes for bacterial detection, Bioelectrochemistry, 86 (2012) 30-37.
[29] G. Ciric-Marjanovic, L. Dragicevic, M. Milojevicl , M. Mojovicl , S. Mentus, B. Dojcinovic, B. Marjanovic, J. Stejskal, Synthesis and characterization of self-assembled polyaniline nanotubes/silica nanocomposites, J. Phys Chem. B, 113 (2009) 7116-7127.
[30] L. Ren, G. Zhang, Z. Yan, L. Kang, H. Xu, F. Shi, Z. Lei, Z.-H. Liu, Three-dimensional tubular MoS_2/PANI hybrid electrode for high rate performance supercapacitor, ACS appl. mater. interfaces 7 (2015) 28294-28302.
[31] M. Kim, Y.K. Kim, J. Kim, S. Cho, G. Lee, J. Jang, Fabrication of a polyaniline/MoS 2 nanocomposite using self-stabilized dispersion polymerization for supercapacitors with high energy density, RSC Adv., 6 (2016) 27460-27465.
[32] A. Soni, C.M. Pandey, S. Solanki, G. Sumana, One-pot synthesis of a polyaniline-gold nanocomposite and its enhanced electrochemical properties for biosensing applications, RSC Adv., 5 (2015) 45767-45774.
[33] D. Wang, K. Zhou, M. Sun, Z. Fang, X. Liu, X. Sun, Room temperature elemental mercury sensor using MoS 2-PANI nano-sheet-flowers composite, Anal. Methods, 5 (2013) 6576-6578.
[34] H. Liu, F. Zhang, W. Li, X. Zhang, C.-S. Lee, W. Wang, Y. Tang, Porous tremella-like MoS_2/polyaniline hybrid composite with enhanced performance for lithium-ion battery anodes, Electrochim. Acta, 167 (2015) 132-138.
[35] C.M. Pandey, G. Sumana, K.N. Sood, B.D. Malhotra, Electrochemical studies of cystine modified self-assembled monolayer for Escherichia coli detection, Thin Solid Films, 519 (2010) 1178-1183.

[36] A. Kaushik, P.R. Solanki, K. Kaneto, C.G. Kim, S. Ahmad, B.D. Malhotra, Nanostructured iron oxide platform for impedimetric cholesterol detection, Electroanalysis, 22 (2010) 1045-1055.
[37] A. Soni, C.M. Pandey, S. Solanki, G. Sumana, Synthesis of 3D-coral like polyaniline nanostructures using reactive oxide templates and their high performance for ultrasensitive detection of blood cancer, Sens. Actuators B: Chem., 281 (2019) 634-642.
[38] C.M. Pandey, I. Tiwari, G. Sumana, Hierarchical cystine flower based electrochemical genosensor for detection of Escherichia coli O157: H7, RSC Adv., 4 (2014) 31047-31055.

Figure Captions

Figure 1. Schematic illustration for the synthesis of (A) Fe_2O_3 nanospindles. (B) Polyaniline nanospindles using Fe_2O_3 templates (C) PANI-MoS_2 nanocomposite. (D) TEM image of Fe_2O_3 nanospindles (E) HRTEM image of Fe_2O_3 nanospindles. TEM images of PANI nanospindles (F) at lower magnification (G) at higher magnification. TEM images of PANI-MoS_2 nanocomposite (H) at lower magnification (I) at higher magnification.

Figure 2. X-Ray Diffraction patterns of (A) PANI-NS (B) PANI-MoS_2 nanocomposite. (C) Raman spectra of (i) PANI-NS (ii) PANI-MoS_2 nanocomposite. DLS measurements representing zeta potential values of (D) PANI-NS (E) PANI-MoS_2 nanocomposite.

Figure 3. Schematic illustration of (A) Electrophoretic deposition of PANI-MoS_2 nanocomposite on ITO electrode and fabrication of pDNA/PANI-MoS_2/ITO bioelectrode. SEM images of (B) PANI-NS/ITO electrode (C) PANI-MoS_2/ITO electrode (inset representing the image at higher magnification) (D) Energy dispersive X-ray spectra of PANI-MoS_2/ITO electrode. (E) SEM image of pDNA/PANI-MoS_2/ITO bioelectrode.

Figure 4. Nyquist diagram for the Faradic impedance of (A) (i) PANI-MoS_2/ITO electrode (ii) PANI-NS/ITO electrode (iii) pDNA/PANI-MoS_2/ITO bioelectrode (B) EIS response of pDNA/PANI-MoS_2/ITO bioelectrode as a function of cDNA concentration (10^{-17} to 10^{-6} M) (C) Linearity relation curve between ΔR_{ct} and log of concentrations of cDNA for pDNA/PANI-MoS_2/ITO bioelectrode (D) EIS response of pDNA/PANI-MoS_2/ITO bioelectrode (i) with (ii) non-complementary (iii) one-base mismatch (iv) CML positive patient sample1 (v) complementary (vii) CML positive patient sample 2.

Figure 1.

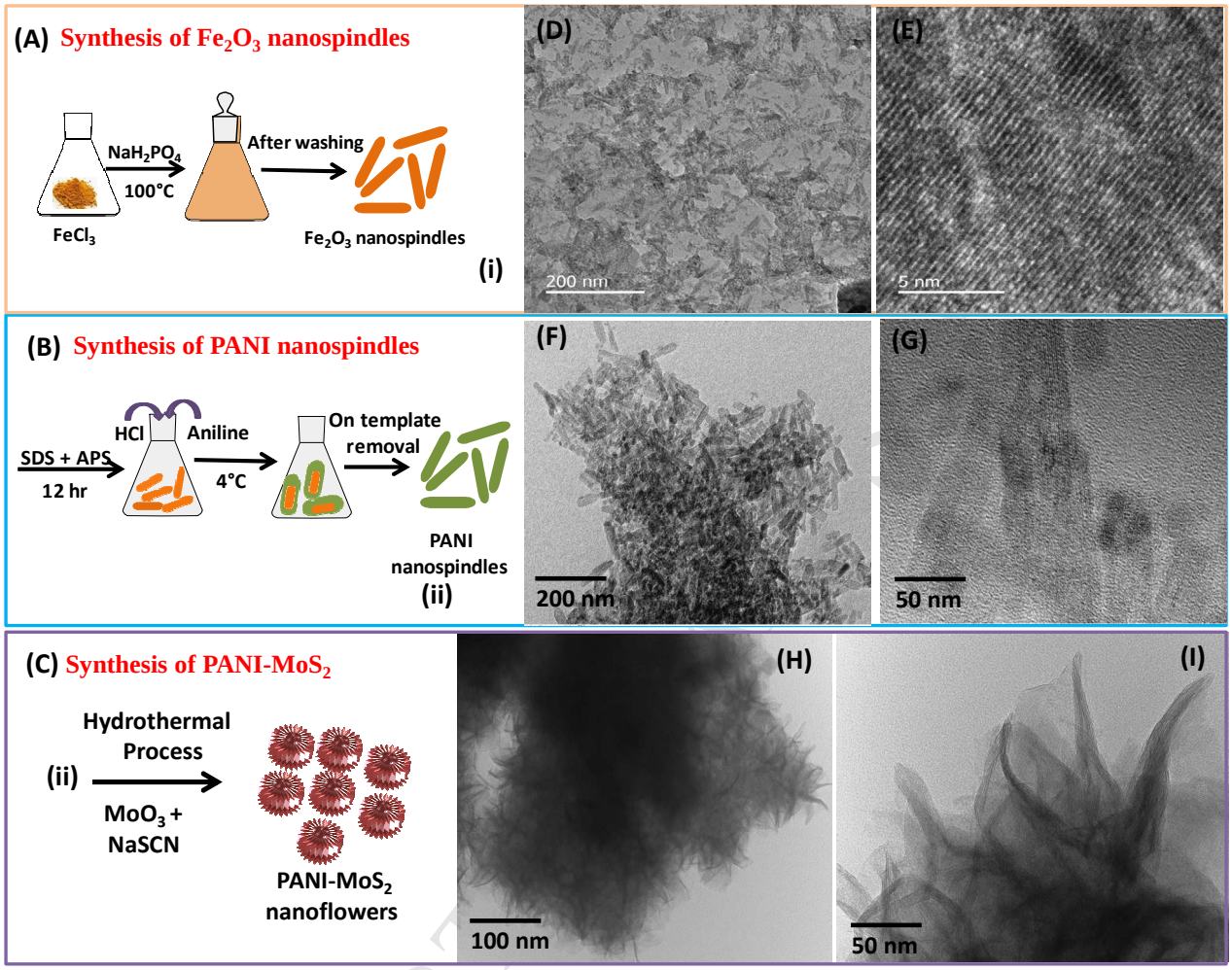
(A) Synthesis of Fe_2O_3 nanospindles
NaH_2PO_4
100°C
After washing
$FeCl_3$
Fe_2O_3 nanospindles
(i)
(B) Synthesis of PANI nanospindles
HCl
Aniline
SDS + APS
12 hr
4°C
On template removal
PANI nanospindles
(ii)
(C) Synthesis of PANI-MoS_2
Hydrothermal Process
(ii)
MoO_3 + NaSCN
PANI-MoS_2 nanoflowers
(D)
200 nm
(E)
5 nm
(F)
200 nm
(G)
50 nm
(H)
100 nm
(I)
50 nm

Figure 2.

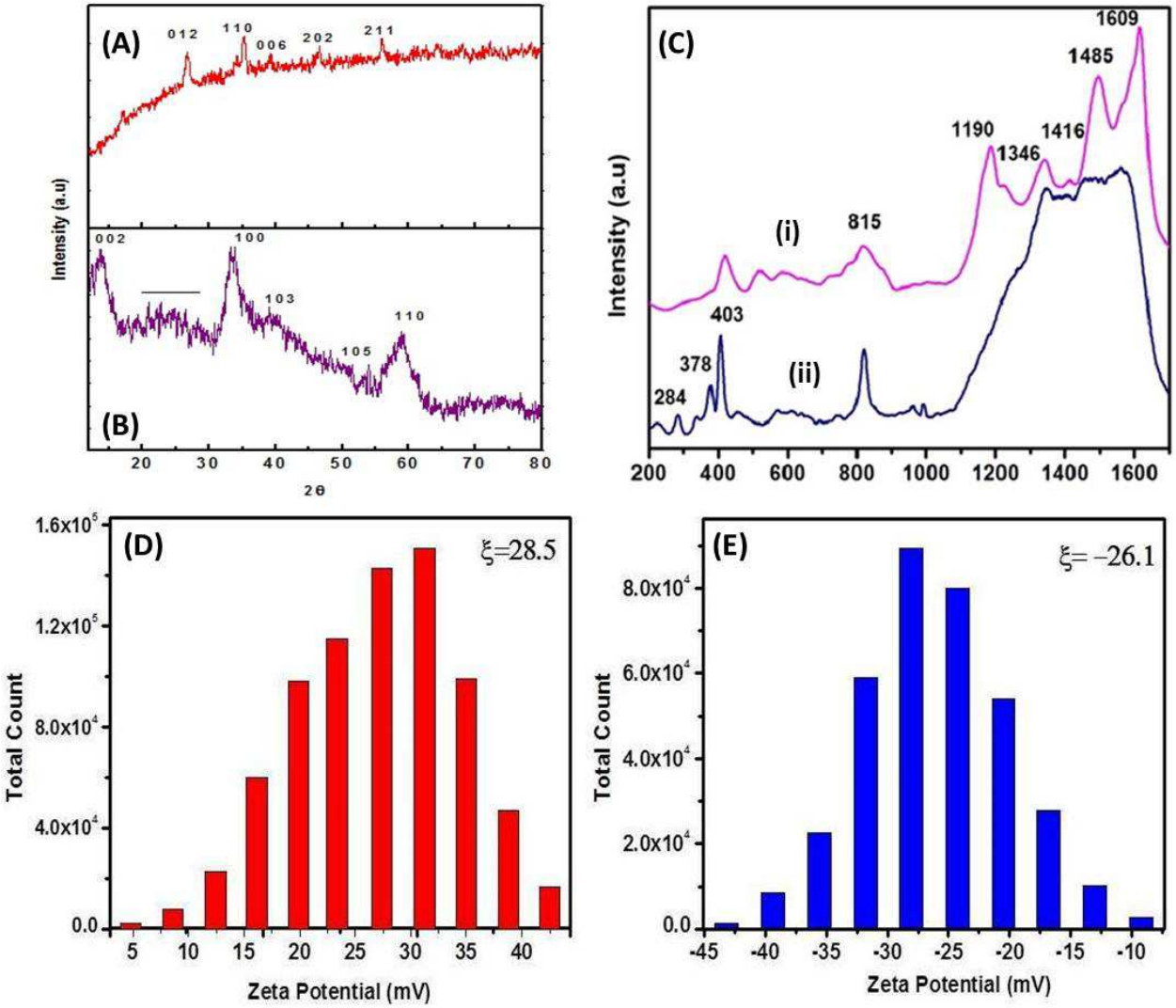
(A)
012
110
006
202
211
002
100
103
110
105
(B)
Intensity (a.u)
2θ
(C)
1609
1485
1190
1416
1346
815
(i)
403
378
284
(ii)
Intensity (a.u)
(D)
ξ=28.5
Total Count
Zeta Potential (mV)
(E)
ξ= –26.1
Total Count
Zeta Potential (mV)

Figure 3.

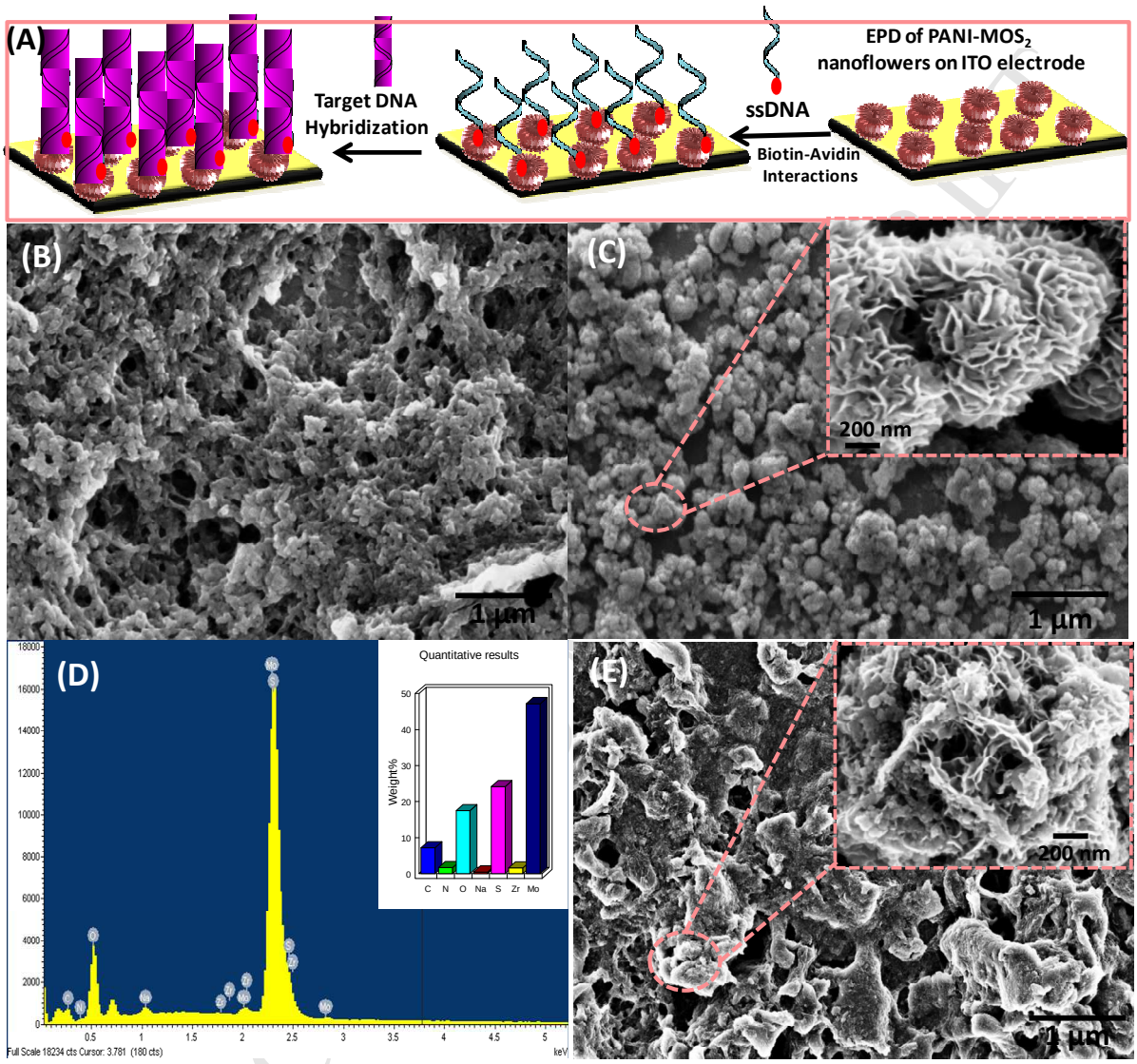
(A)
Target DNA
Hybridization
ssDNA
Biotin-Avidin
Interactions
EPD of PANI-MOS2
nanoflowers on ITO electrode
(B)
1 µm
(C)
200 nm
1 µm
(D)
Quantitative results
Weight%
C N O Na S Zr Mo
Full Scale 18234 cts Cursor: 3.781 (180 cts)
keV
(E)
200 nm
1 µm

Figure 4.

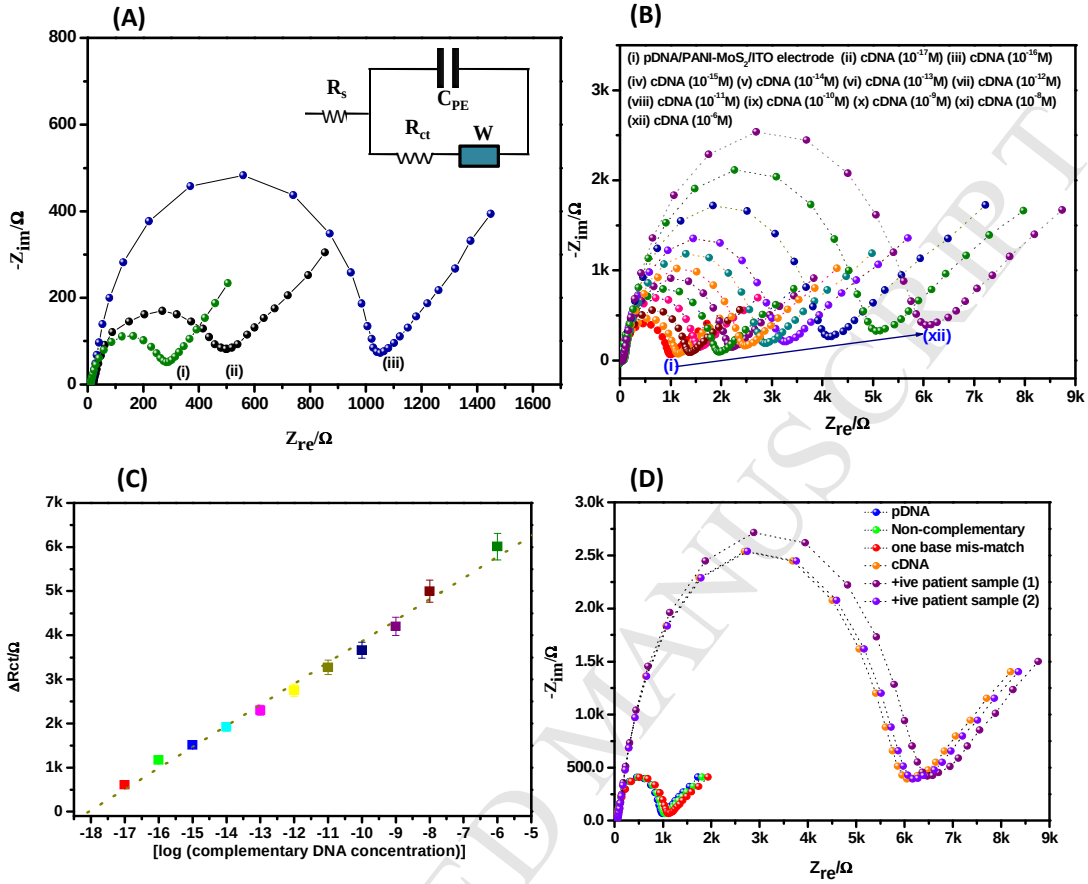

Highlights

- Synthesis of uniform 3D PANI-MoS_2 hybrid nanostructures.
- Deposition of PANI-MoS_2 onto ITO substrate enhances electrochemical performance.
- Label-free, selective and ultrasensitive (3×10^{-18}M) biosensor for CML detection.
- Validation with clinical samples shows its great potential in cancer diagnosis.